Vector dither experiment design and direct parametric identification of reversed-field pinch normal modes

Erik Olofsson[1], Håkan Hjalmarsson[2], Cristian Rojas[2], Per Brunsell[1] and James Drake[1]

Abstract— Magnetic confinement fusion (MCF) research ambitiously endeavours to develop a major future energy source. MCF power plant designs, typically some variation on the *tokamak*, unfortunately suffer from *magnetohydrodynamic* (MHD) instabilitites. One unstable mode is known as the *resistive-wall mode* (RWM) wich is a macroscopically *global* type of perturbation that terminates the plasma in the reactor if not stabilized. In this work the topic of RWMs is studied for the *reversed-field pinch* (RFP), another toroidal MCF concept, similar to the tokamak. The problem of identifying RWM dynamics during closed-loop operation is tackled by letting physics-based parametric modeling join forces with convex programming experiment design. An established MHD *normal modes* description is assessed for the RFP by synthesizing a multivariable dither signal where spatial fourier modes are spectrally shaped, with regard to real experiment constraints, to yield minimum variance parameter estimates in the prediction-error framework. The dithering is applied to the real RFP plant EXTRAP-T2R, and experimental MHD spectra are obtained by an automated procedure.

I. INTRODUCTION

Commercial-grade thermonuclear fusion reactors, the positive forecasts say, could get on-line on the power grid in about 30-40 years from this date. A fusion reactor is a serious technological and scientific undertaking and whether the prognosis is heartwarmingly optimistic or conservative is to a large extent decided by the outcome of the ITER (international thermonuclear experimental reactor) [1] project, being built in Cadarache, France. Naturally, financial and political kudos for fusion engineering research ultimately hinge on a non-ambiguous demonstration of real power-generating experimental results, viz. the task of ITER, as it aims for 500 MW net output.

Now, ITER is a *tokamak* design [2], meaning it has a toroidal geometry and thus resembles a bagel, or a doughnut. A tokamak works in accordance with magnetic confinement fusion (MCF) principles; the exceptionally hot ionized gas (order 10^7 K) is kept away from the interior vessel walls since charged particles are $\mathbf{v} \times \mathbf{b}$-deflected by magnetic field lines. This magnetic field must be cleverly engineered to ensure stability of the *plasma*. For tokamaks the field is generated by *i)* strong external electromagnets (neccessarily superconducting in the ITER case) and *ii)* the inductive electrical current in the plasma itself. Combined, the field is twisted along the toroidal direction, forming a 'magnetic cocoon' able to sustain fusion-quality plasmas, supposedly. Indeed, the regime of fusion plasma conditions is still

peppered with bold-fonted question-marks, of which many deserve attention from and pose challenges to automatic control experts [3].

In this work we are considering a particular MCF devise known as the *reversed-field pinch* (RFP). RFPs are closely related to tokamaks. Specifically, we here treat the *resistive-wall mode* (RWM) *instability*, relevant to both machines, but easier to study in the RFP. The RWM could turn out to be a limiting factor for tokamak reactor operation, so its understandning and stabilization is a high priority issue.

The study here aims to contribute to the topic of RWMs in particular but also to magnetic plasma control in general. We are assessing a structured and parametric RFP model for RWMs and this is triple-purpose: *a)* experimental magnetohydrodynamic (MHD) [4] stability research *b)* prospecting identification for control and reconfiguration of stabilizing circuit and *c)* development of identification methods and perturbation designs for MCF research. Take a note of the wide span of this novel collaborative work: modeling, identification, input-design, real-world implementation and conduction of the true physical experiment; reflecting the possibilities for new ideas and progression in control-oriented MCF.

Our presentation is organized as follows. The RFP plant and the physics-based parameterizations are inaugurated in section II. System identification method and dither-design synthesis are respectively explained in sections III and IV. Section V presents experimental results and the paper is ended with concluding commentaries in section VI.

II. EXTRAP-T2R AND MODAL PARAMETRIC MODELING

A. EXTRAP-T2R

At the time of writing, only three actively running RFP experiments exists worldwide. The smallest is EXTRAP-T2R in Stockholm, Sweden. It is very well equipped for MHD control studies due to its' dense arrays of sensor and active coils combined with a thin conducting wall allowing instabilities to develop fully during the experiment. T2R have demonstrated the feasibility [5], [6] to stabilize multiple RWMs by intelligent-shell-type (IS) feedback [7], as defined below.

T2R real-time feedback control, for this study, involves 64 inputs and 64 outputs, and a sample-interval $T_s = 100\,\mu$s. However the linearized dynamics of perturbations to the cylinder-symmetric MHD equilibrium for RFPs is believed to be reasonably well-described by an independent normal modes model [8], [9], [10]. As it happens, it is then possible

to decouple the MIMO plant into a list of SISO systems each involving an infinite number of superimposed *spatially aliased* independent MHD modes. Theoretically only a handfull of these contributing modes are important (unstable, marginally stable), but to interpret the signals correctly a larger set of modes need be accounted for.

We can write the independent modes' response [11], [8]

$$\tau_{m,n}\dot{x}_{m,n} - \hat{\gamma}_{m,n}x_{m,n} = x_{m,n}^{app} + x_{m,n}^{fe}, \ \forall m > 0, n \in \mathbb{Z} \tag{1}$$

where $x_{m,n}$ is the state of the MHD mode (m,n), $\tau_{m,n}$ a modal time-constant, $\hat{\gamma}_{m,n}$ the normalized growth-rate of the mode (to $\tau_{m,n}$), and $x_{m,n}^{app}$ the externally applied magnetic field generated from the control input. The additional driving term $x_{m,n}^{fe}$ is called *field-error* in this work. Subsection II-D below develops a truncation and discrete-time parametric representation of (1); the fundamental ingredient of this investigation, summarized in form (6).

Figure (1) depicts a clean $(m = 1, |n| = 5)$ periodic cylinder plasma perturbation. The (m,n)-enumeration should be understood as follows. Betokening an MHD-equilibrium magnetic field $\mathbb{R}^3$-vector perturbation $\mathbf{b}_{m,n}(r,t)$ where r is the cylindrical radial coordinate we have $\mathbf{b}_{m,n}(r,t) = \mathbf{b}_{m,n}(r)e^{\iota(\omega t + m\theta + n\phi)}$ and $x_{m,n} = \mathbf{b}_{m,n}(r_w,t) \cdot \hat{\mathbf{r}}$, using θ, ϕ for poloidal and toroidal angles respectively.
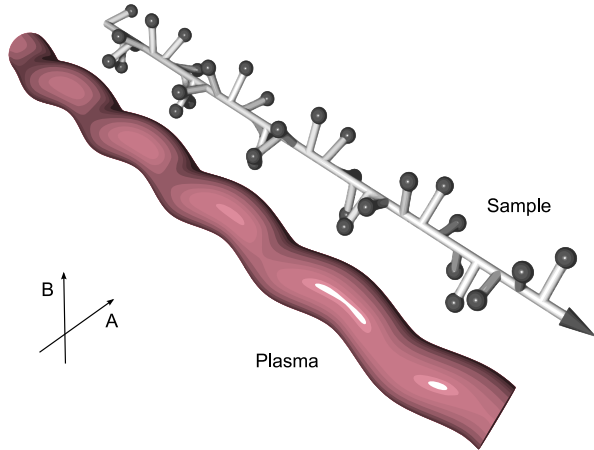
B. Signal vector notation and IS stabilization

Fig. 1. Contorted plasma column and its 32-point vector-sample representation $\bar{\mathbf{y}}(t)$.

Let $\bar{\mathbf{s}}(t)$ denote either of the vector signals $\bar{\mathbf{u}}(t)$, $\bar{\mathbf{y}}(t)$, $\bar{\mathbf{w}}(t)$, each representing the physical channels of the plant: active coil currents, measured magnetic fields, and channel dither inputs, respectively. All these vectors have 64 components so $\bar{\mathbf{s}}(t) \in \mathbb{R}^{64}$. For any toroidal position $j = 0 \ldots 31$ pick out the outboard-inboard A and top-down B signal by indexing $\bar{s}_{j,A}(t)$ and $\bar{s}_{j,B}(t)$. The signal $\bar{\mathbf{y}}(t)$ is graphically illustrated in figure 1. We relate $\bar{\mathbf{s}}$ to spatial fourier vector

$\mathbf{s}(t)$ in this way:

$$(\mathcal{T}\bar{\mathbf{s}})_i(t) = \sum_{j=0}^{N-1} W_{ji}\left(\bar{s}_{j,A}(t) + \iota\bar{s}_{j,B}(t)\right)$$

$$s_j(t) = \begin{cases} \text{Re }(\mathcal{T}\bar{\mathbf{s}})_j(t), \ j = 0 \ldots 31 \\ \text{Im }(\mathcal{T}\bar{\mathbf{s}})_{j-32}(t), \ j = 32 \ldots 63 \end{cases} \tag{2}$$

where $\iota^2 = -1$ and $W_{ji} = e^{-2\pi j i\iota/N}$, and $N = 32$. Bold $\mathbf{s}(t) \in \mathbb{R}^{64}$ is then simply constituted by components $s_j(t)$. Introducing $\mathbf{n}^T = (0 \ldots 15, -16 \ldots 15, -16 \ldots -1)$ allows the relation between mode-number n and vector index j of s_j to be expressed: $n(j) = n_j$, n_j the jth component of $\mathbf{n}$.

The IS stabilization [7] is the *decentralized* feedback-law of form

$$\bar{u}'_{j,A}(t) = C(s)(\bar{r}_{j,A}(t) - \bar{y}_{j,A}(t)) + \bar{w}_{j,A}(t) \tag{3}$$

where $\bar{u}'_{j,A}(t)$ is the voltage input to the bundled peripheral dynamic $F(s)$, detailed in subsection II-C, such that $\bar{u}_{j,A}(t) = F(s)\bar{u}'_{j,A}(t)$. Substitute A for B in (3) to complete the IS feedback strategy.

Note carefully that the vector dither $\bar{\mathbf{w}}$ synthesized below enter the plant through (3). This synthesis is performed for each fourier dither component $w_j(t)$ *independently*, and subsequently the inverse of (2) yields $\bar{\mathbf{w}}(t)$.

C. Peripheral dynamics

For the purpose of experiment design, section IV, descriptions of systems F and C in figure 2 are required

$$F(s) = \frac{\tau_1 s}{\tau_1 s + 1}\frac{K}{\tau_2 s + 1}$$
$$C(s) = k_p + \frac{k_i}{s} + \frac{k_d s}{k_d s/N_d + 1} \tag{4}$$

$F(s)$ and $C(s)$ are zero-order-hold discretized and subsequently inserted in the input-design programs of section IV. Again, identification is *direct* hence approximations (4) do not flaw estimated parameters other than perhaps slightly mis-shaping the applied dither, giving suboptimal variance.

Numerically, we use $\tau_1 = 0.10\,\text{s}$, $\tau_2 = 1.0\,\text{ms}$, $K = 4.1$, $k_p = 40$, $k_i = 5000$, $k_d = 0.04$, and $N_d = 30$. Numbers originate from [6].

D. Parametric SISO modeling ansatz with incorporated noise

This section details a process model

$$y_i(t) = G_i(q,\theta_i)u_i(t) + H_i(q,\theta_i)e_i(t) \tag{5}$$

relating *direct* input-output of the T2R plant $G_i(q,\theta_i)$ in fourier space, $e_i(t)$ being a white sequence driving the process noise $H_i(q,\theta)e_i(t)$. q^{-1} conventionally denotes a delay operator $q^{-1}x(t) = x(t - T_s)$. Discretizing linear RWM-dynamics (1) and accounting for discrete-array spatial aliasing for T2R geometry results in the ith SISO model

$$G_i(q,\theta_i) = \sum_{(m,n)\in\mathcal{K}_{n(i)}} G_{m,n}(q,\theta_i) \tag{6}$$

where

$$G_{m,n}(q,\theta) = \frac{\alpha \hat{c}_{m,n} \hat{b}_{m,n} \frac{1}{\hat{\gamma}_{m,n}} \left(\hat{d}_{m,n} - 1 \right) q^{-1}}{1 - \hat{d}_{m,n} q^{-1}} \qquad (7)$$

using $\hat{d}_{m,n} = e^{\frac{\hat{\gamma}_{m,n} T_s}{\hat{\tau}_{m,n\tau}}}$. In this work we will *only* consider the truncation

$$\mathcal{K}_n = \left\{ \begin{array}{ll} (1,n), & (1,n-32),(1,n+32), \\ (3,n), & (3,n-32),(3,n+32), \\ (5,n), & (5,n-32),(5,n+32) \end{array} \right\} \qquad (8)$$

which seems adequate for (practical) T2R studies. In addition to (6) and (7) we will impose a structure

$$H_i^{fe}(q,\theta_i) = \frac{b_i q^{-1}}{1 - a_i q^{-1}} \qquad (9)$$

to append (6) forming the noise model

$$H_i(q,\theta_i) = G_i(q,\theta_i) H_i^{fe}(q,\theta_i) \qquad (10)$$

In the above, given constants are

$$\hat{c}_{m,n} = c_0 \frac{1}{mn} \sin(m\delta\theta/2) \sin(n\delta\phi/2) \qquad (11)$$

$$\hat{b}_{m,n} = b_0 \frac{n}{m} \sin(m\Delta\theta/2) \sin(n\Delta\phi/2)$$
$$\times K'_m(|n|r_c/R) I'_m(|n|r_w/R) \qquad (12)$$

$$\hat{\tau}_{m,n} = \frac{1}{4} \left(1 + \frac{m^2}{n^2 \epsilon_r^2} \right)^{-1} K'_m(|n|\epsilon_r) I'_m(|n|\epsilon_r) \qquad (13)$$

where $\epsilon_r = r_w/R$, normalizations b_0, c_0 such that $\hat{b}_{1,1} = \hat{c}_{1,1} = 1$ and I'_m and K'_m are bessel functions[1] derivatives, and $\epsilon_r = r_w/R$. T2R measures: coils' angular dimensions $\delta\theta = \Delta\theta = \frac{2\pi}{4}$, $\delta\phi = \frac{2\pi}{64}$, $\Delta\phi = \frac{2\pi}{32}$, major toroidal radius $R = 1.24\,\mathrm{m}$, active coil minor radial position $r_c = 0.235\,\mathrm{m}$, and resistive-shell radial position $r_w = 0.198\,\mathrm{m}$.

1) Partitioned parameter vector θ_i: Equations (5), (6), (10) summarize the structure imposed. Nominally, the parameter vector reads $\theta_i = \begin{pmatrix} \alpha_i & \tau_i & \hat{\gamma}_i & a_i & b_i \end{pmatrix}^T$, but identification is split into different parts as follows.

$$\theta_i = \begin{pmatrix} \theta_{i,dry}^T & \theta_{i,wet} & \theta_{i,ofs}^T \end{pmatrix}^T$$
$$\begin{cases} \theta_{i,dry} = \begin{pmatrix} \alpha_i & \tau_i \end{pmatrix}^T \\ \theta_{i,wet} = \hat{\gamma}_i \equiv \hat{\gamma}_{m=1,n=n(i)} \\ \theta_{i,ofs} = \begin{pmatrix} a_i & b_i \end{pmatrix}^T \end{cases} \qquad (14)$$

First stage of partitioning (14) is to deal with open-loop acquired vacuum (dry) data and to enforce $\forall m,n : \hat{\gamma}_{m,n} \equiv -1$, as this means exactly 'no plasma' for plant (6), allowing identification of $\theta_{i,dry}$. This does *not* involve the process noise (10); figure 2(a). Using data from prior experiments on the plasma plant (wet) we then *fix* subvector $\theta_{i,ofs}$ by estimating (9) from batch-averaged signals $\langle u_i \rangle(t) = \frac{1}{|\mathcal{E}|} \sum_{j \in \mathcal{E}} u_i^{(j)}(t)$, $\mathcal{E}$ denoting a batch of experiments, $|\mathcal{E}|$ the number of experiments in this batch and $u_i^{(j)}(t)$ recorded $u_i(t)$ for experiment j in $\mathcal{E}$, for component i of $\mathbf{u}(t)$. This

[1]*modified* Bessel functions of the *first*, I and *second* K, kinds

step sketches field-error spectral densities (mostly a relatively slow 'drift'). Finally, the remaining scalar parameter $\theta_{i,wet}$ is estimated from new experiments, specifically designed from the other parts $\theta_{i,dry}$ and $\theta_{i,ofs}$, as detailed in section IV.

We should emphasize an important simplification in the above parameterization: each mode belonging to (8) technically has its own growth-rate for the wet plant, but $\theta_{i,wet}$ only include the particular $\hat{\gamma}_{m=1,n(i)}$. All other modal growth-rates are confined to their dry level $\hat{\gamma}_{m,n} = -1$ in this work, an approximately true fact in theory: the $m = 1$-branch is dominating in RFPs [8], with the marginal and unstable modes accumulated at low-$|n|$.

E. Loop schematics

Figure 2 should be interpreted in the spatial fourier domain such that scalar signals w, u and y represents the components w_j, u_j, y_j for some j. The routings are approximate in the sense that the feedback is *not* operating in this domain, but rather in 'real' channel space $\bar{w}_i$, $\bar{u}_i$, $\bar{y}_i$. However the IS setup is designed to give as equal response at each spatial location as possible, so the approximation with single $F(s)$ and $C(s)$ is reasonable for dither input-design.
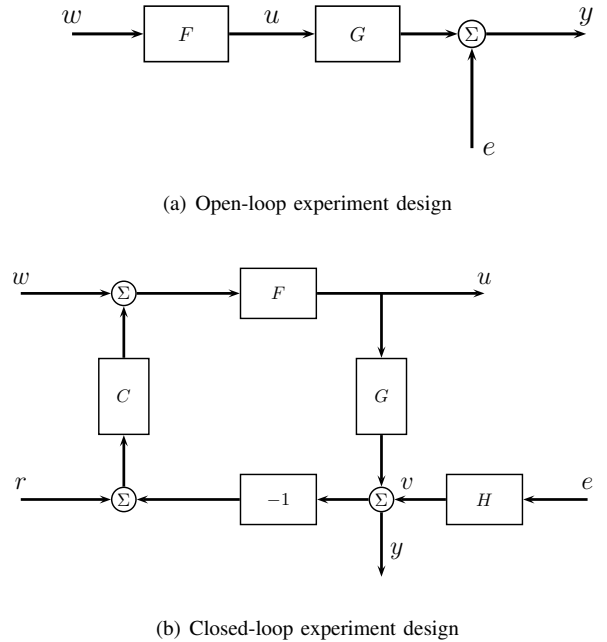

(a) Open-loop experiment design

(b) Closed-loop experiment design

Fig. 2. Schematics of experiment set-ups for dry and wet plant respectively. Objective in both cases is to shape spectrum $\Phi_w(\omega)$.

III. DIRECT PREDICTOR-BASED NORMAL-MODES IDENTIFICATION

The identification problem [12] for a parameterized SISO discrete-time time-invariant system

$$\mathbf{x}(k+1) = A(\theta)\mathbf{x}(k) + B(\theta)u(k) + \mathbf{z}(k)$$
$$y(k) = C(\theta)\mathbf{x}(k) + v(k) \qquad (15)$$

where $\mathrm{E}v(k_1)v(k_2) = \delta_{k_1-k_2}R$, $\mathrm{E}\mathbf{z}(k_1)\mathbf{z}^T(k_2) = \delta_{k_1-k_2}Q$ with E the expectation operator, can be cast as a program

$$\theta^\star = \arg\min_\theta V(\theta) \qquad (16)$$

where $V(\theta) \equiv \frac{1}{N}\sum_{k=1}^{N}e^2(k,\theta)$ and the *prediction errors* $e(k,\theta) \equiv y(k) - \hat{y}(k,\theta)$ are produced by a *predictor* $\hat{y}(k,\theta) = f\left(\theta, \{y(l), u(l)\}_{l=0,\dots,k-1}\right)$. Solving (16) yields an *identified* model (15) $(A(\theta^\star), B(\theta^\star), C(\theta^\star))$. As is well known [12], [13], this method applies to data acquired from systems operating in closed-loop.

A. Direct identification program

We employ the following recursive predictor algorithm [14], [15]

$$\begin{cases} \hat{\mathbf{x}}^-(k) = A\hat{\mathbf{x}}^+(k-1) + Bu(k-1) \\ P^-(k) = AP^+(k-1)A^T + Q \end{cases} \text{(predict)}$$

$$\begin{cases} e^-(k) = y(k) - C\hat{\mathbf{x}}(k)^- \\ K(k) = P^-(k)C^T\left(CP^-(k)C^T + R\right)^{-1} \\ \hat{\mathbf{x}}^+(k) = \hat{\mathbf{x}}^-(k) + K(k)e^-(k) \\ P^+(k) = (I - K(k)C)P^-(k) \end{cases} \text{(update)}$$

$$(17)$$

where the prediction error output is $e(k,\theta) \equiv e^-(k)$. Although time-invariant identification is considered (P^-, P^+ and K are known to converge to precomputable values) we keep the full format of the *kalman* one-step-predictor (17) to be able to express lack of knowledge of initial state $\hat{\mathbf{x}}^+(0)$, i.e. $P^+(0)$ large, and use a burn-in phase not included in the prediction-error value.

B. State-space augmentation for wet plant

Let $(A(\theta_{i,dry}), B(\theta_{i,dry}), C(\theta_{i,dry}))$ denote the state-space representation of (6) in the sense (15). A wet plant state-space augmentation is then

$$A(\theta_{i,wet}) = \begin{pmatrix} A(\theta_{i,dry}) & \frac{b_i}{\alpha_i}B(\theta_{i,dry}) \\ 0 & a_i \end{pmatrix}$$

$$B(\theta_{i,wet}) = \begin{pmatrix} B(\theta_{i,dry}) \\ 0 \end{pmatrix} \qquad (18)$$

$$C(\theta_{i,wet}) = \begin{pmatrix} C(\theta_{i,dry}) & 0 \end{pmatrix}$$

IV. CONVEX PROGRAMMING EXPERIMENT DESIGN

This section aims to design an excitation signal [16] to plant (6) such that acquired data is rich in information with respect to the (partially) unknown parameters of (6). Metaphorically speaking, spoonfeeding program (16) with liberal servings of healthy data sprouts distinct parameters (provided the model is correct). This is achieved by distinguishing *a)* open-loop experiment (subsection IV-C) for the dry system *b)* closed-loop stabilized experiment (subsection IV-D) for the wet system.

A. Experiment design prerequisities

In the prediction-error framework the following basic result in input-design can be found.

$$P^{-1}(\theta_0) = \frac{1}{2\pi\lambda_0}\int_{-\pi}^{\pi}\mathcal{F}(e^{\iota\omega})\Phi_{\chi_0}(\omega)\mathcal{F}^*(e^{\iota\omega})d\omega \qquad (19)$$

where $\mathcal{F} = \begin{pmatrix} F_u & F_e \end{pmatrix}$, $F_u = H^{-1}\frac{\partial G}{\partial\theta}$, $F_e = H^{-1}\frac{\partial H}{\partial\theta}$, and $\Phi_{\chi_0} = \begin{pmatrix} \Phi_u & \Phi_{ue} \\ \Phi_{ue}^* & \lambda_0 \end{pmatrix}$. Equation (19) relates the model parameter estimate (inverse) covariance matrix to the input spectrum $\Phi_u(\omega)$ and the model itself $y = G(q,\theta_0)u + H(q,\theta_0)e$ with $\mathrm{E}e(k+l)e(k) = \delta_l\lambda_0$.

For this study we are content to minimize variance of estimates given a limit on the input power. In short, the program

$$\min_{\phi_u}\mathrm{tr}\,WP, \text{ s.t. } \frac{1}{2\pi}\int_{-\pi}^{\pi}\Phi_u(\omega)d\omega \le \beta \qquad (20)$$

could be solved to achieve this. Below (20) is instantiated for open- and closed-loop operation of T2R using a special dither input w. Note that (20) equivalently can be rephrased as

$$\min_{\phi_u, Z}\mathrm{tr}\,Z \text{ s.t. } \begin{cases} \frac{1}{2\pi}\int_{-\pi}^{\pi}\Phi_u(\omega)d\omega \le \beta \\ \begin{pmatrix} Z & V \\ V^* & P^{-1} \end{pmatrix} \ge 0 \end{cases} \qquad (21)$$

using a Schur complement [17] where $0 \le W = VV^*$ and any affine parameterization of Φ_{χ_0} now generates a linear matrix inequality (LMI) constraint involving the matrix slack variable $Z = Z^T \in \mathbb{R}^{n\times n}$, $\dim\theta = n$.

For $\Phi_{ue} = 0$ inverse covariance (19) collapses to

$$P^{-1}(\theta_0) = \frac{1}{2\pi\lambda_0}\int_{-\pi}^{\pi}F_u\Phi_u F_u^* d\omega + \frac{1}{2\pi}\int_{-\pi}^{\pi}F_e F_e^* d\omega \qquad (22)$$

which is often sufficient for open-loop systems (and fixed-controller systems). We will exclusively utilize (22) in the experiment designs below.

B. Finite parameterization and realization of spectrum

A spectrum parameterization of order M, defined by real-valued coefficients $\{r_i\}_{i=0}^{M-1}$ is

$$\Phi_w(\omega) = \sum_{k=-(M-1)}^{M-1} r_{|k|}e^{-\iota\omega k} = r_0 + 2\sum_{k=1}^{M-1} r_k\cos(k\omega) \qquad (23)$$

Introducing the matrices

$$A_w = \begin{pmatrix} 0_{1\times(M-2)} & 0 \\ I_{M-2} & 0_{(M-2)\times 1} \end{pmatrix} \quad B_w = \begin{pmatrix} 1 \\ 0_{(M-2)\times 1} \end{pmatrix}$$

$$C_w = \begin{pmatrix} r_1 & r_2 & \dots & r_{M-1} \end{pmatrix} \quad D_w = \frac{1}{2}r_0 \qquad (24)$$

conveniently allows the spectrum constraint $\Phi_w(\omega) \ge 0$ to be expressed by LMI feasibility in $Q = Q^T \in \mathbb{R}^{(M-1)\times(M-1)}$

$$\exists Q: \begin{pmatrix} Q - A_w^T Q A_w & C_w^T - A_w^T Q B_w \\ C_w - B_w^T Q A_w & D_w + D_w^T - B_w^T Q B_w \end{pmatrix} \ge 0 \qquad (25)$$

Having obtained a set of parameters $\{r_i\}$ passing (25) an M-tap finite impulse response (FIR) filter can be calculated through spectral factorization [14] as follows. Solve the discrete-time algebraic Riccati equation $X = A_w X A_w^T - (A_w X C_w^T - B_w) \times (C_w X C_w^T - D_w - D_w^T)^{-1} \times (A_w X C_w^T - B_w)^T$ then put $\Omega_w = D_w + D_w^T - C_w X C_w^T$ and $K_w = -(A_w X C_w^T - B_w)/\Omega_w$ to find a state-space FIR realization $(A_w, K_w, \sqrt{\Omega_w} C_w, \sqrt{\Omega_w})$.

C. Design for identification of dry plant: open-loop

Straighforward application of open-loop input design theory using a (white) noise model $H_i(q, \theta_i) \equiv 1$ on the peripheral-augmented plant $G_i(q, \theta_i)F(q)$ (situation depicted in figure 2(a)), where i indexes the plant model, yields the convex program

$$\min_{Z, Q, \{r_j\}_{j=0}^{M-1}} \operatorname{tr} Z$$
$$\text{s.t.} \begin{cases} \dfrac{1}{2\pi} \displaystyle\int_{-\pi}^{\pi} \Phi_w(\omega)d\omega = r_0 \le \beta_{i,OL} \\ \begin{pmatrix} Z & V \\ V^* & P^{-1} \end{pmatrix} \ge 0 \\ \begin{pmatrix} Q - A_w^T Q A_w & C_w^T - A_w^T Q B_w \\ C_w - B_w^T Q A_w & D_w + D_w^T - B_w^T Q B_w \end{pmatrix} \ge 0 \end{cases}$$
$$(26)$$

where

$$P^{-1}(\theta_i^{(0)}) = \frac{1}{2\pi\lambda_0} \int_{-\pi}^{\pi} \frac{\partial G}{\partial \theta} \frac{\partial G^*}{\partial \theta} \bigg|_{\theta=\theta_i^{(0)}} |F(e^{\iota\omega})|^2 \Phi_w(\omega)d\omega \tag{27}$$

and $\theta_i^{(0)} = \theta_{i,dry}^{(0)}$, (0) meaning the best known guess so far. Optimal spectrum $\Phi_{w_i}^*$ is realized as explained in subsection IV-B.

D. Design for identification of wet plant: closed-loop

We use open-loop input design results for the SISO system (figure 2(b), set $r = 0$)

$$y(t) = G'(q, \theta)w(t) + H'(q, \theta)e(t)$$
$$G'(q, \theta) = \frac{GF}{1 + GFC} \tag{28}$$
$$H'(q, \theta) = \frac{H}{1 + GFC} = \frac{GH^{fe}}{1 + GFC}$$

where the index i is omitted for brevity. When the parameter $\theta = \theta_{i,wet}$ only affect G (neither F, C nor H^{fe})

$$\frac{\partial G'}{\partial \theta} = \frac{\frac{\partial G}{\partial \theta} F}{(1 + GFC)^2} \tag{29}$$

$$\frac{\partial H'}{\partial \theta} = \frac{\frac{\partial G}{\partial \theta} H^{fe}}{(1 + GFC)^2} \tag{30}$$

and so using $F_w = (H')^{-1} \frac{\partial G'}{\partial \theta}$ and $F_e = (H')^{-1} \frac{\partial H'}{\partial \theta}$ we get since $\mathbb{E}w(t)e(t) = 0$

$$P_l^{-1} = \frac{1}{2\pi\lambda_0} \int_{-\pi}^{\pi} \Phi_w \ F_w F_w^* |_{\theta=\theta^{(0,l)}} \ d\omega$$
$$+ \frac{1}{2\pi} \int_{-\pi}^{\pi} F_e F_e^* |_{\theta=\theta^{(0,l)}} \ d\omega \tag{31}$$

by denoting $P^{(-1)}(\theta^{(0,l)}) = P_l^{-1}$. Then component i input design program becomes

$$\min_{z, Q, \{r_j\}_{j=0}^{M-1}} z$$
$$\text{s.t.} \begin{cases} r_0 \le \beta_{i,CL} \\ \begin{pmatrix} z & 1 \\ 1 & P_l^{-1} \end{pmatrix} \ge 0 \ \forall l \text{ such that } \theta^{(0,l)} \in \mathcal{S}_i \\ \begin{pmatrix} Q - A_w^T Q A_w & C_w^T - A_w^T Q B_w \\ C_w - B_w^T Q A_w & D_w + D_w^T - B_w^T Q B_w \end{pmatrix} \ge 0 \end{cases}$$
$$(32)$$

since the parameter is a scalar $\dim\theta = 1$. With (32) there is the ability to approximately design inputs for a *range* of growth-rates as included in the set $\mathcal{S}_i$.

E. Going multivariable: vector dither synthesis

In programs (26) and (32) we can choose an input energy limit $\beta_{i,\cdot}$ according to

$$\beta \le \bar{\beta}(a, \rho, N) = \frac{N^2}{N-1} \left(\frac{a}{f^{-1}(\frac{1}{2}\rho)} \right)^2 \tag{33}$$

in order to enforce the probabilistic signal amplitude constraint

$$\forall j: \ P\left(|\bar{w}_j(t)| \ge a\right) \le \rho \tag{34}$$

when the $n = 0$ spatial DFT component $w_0(t)$ of the input is set to zero. Here $f(\xi) = \int_{-\infty}^{\xi} \frac{1}{\sqrt{2\pi}} e^{-x^2/2} dx$ is the cumulative normal distribution function, $f^{-1}(f(\xi)) = \xi$, and $N = 32$ the DFT size.

In short (33) ensures that the physical channel dithering $\bar{\mathbf{w}}(t)$ at an arbitrary channel index j doesn't saturate the amplitude limit a too often. Albeit a bit fuzzy, this criterion is handy when conducting experiments. We can easily use existing empirical knowledge of what as are good choices and then construct the constraints by setting $\beta = \bar{\beta}(a, \rho \sim 0.01, N = 32)$ according to (33).

V. DEPLOYMENT AND EXPERIMENTAL RESULTS

A. The sequence of experiments

A set of dry experiments and a set of wet experiments had been acquired prior to this work; all using an assortment of PRBS-settings for dithering. This provided an initial parameter guess $\theta_{i,dry}^{(0)}$ as well as fixing $\theta_{i,ofs}^{(0)}$ for this study. The initial estimate $\theta_{i,wet}^{(0)}$ was never used in this work partly because the prior method of identification for this parameter differed subtly.

Solving (26) using $\beta_{i,OL} = \bar{\beta}(5, 0.01, 32)\forall i$, $\lambda_0 = 10^{-2}$ and $M = 8$ then resulted in 64 FIR filters with respective spectrum $\Phi_{w_i}(\omega)$ of form (23) subsequently feeded with unit-variance uniformly distributed random numbers; pregenerating a vector input. The resulting estimates are scatterplotted on top (blue) of the estimates produced from assorted-PRBS batches (green) in fig.3(b). Suffice to say here, the estimates clearly have less variance than previously, and culled outliers.

The new data-set then updated the prior guess $\theta_{i,dry}^{(0)}$ (red circles in fig.3(b)). This new value of $\theta_{i,dry}^{(0)}$ together with our pretended fix-value of $\theta_{i,ofs}^{(0)}$ provided model-input to program (32) using an energy constraint $\beta_{i,CL} = \bar{\beta}(3, 0.01, 32)\forall i$, and $\lambda_0 = 1$. Now the prior guess for the unknown wet-plant parameter was set to $\mathcal{S}_i = \left\{ -\frac{1}{3}, +\frac{1}{3} \right\}$, $\forall i$, i.e. somewhere around marginal stability. Optimized spectra $\Phi_{w_i}(\omega)$ was again $M = 8$-tap realized and prerendered for the experiment. As it turns out, the effect of $\theta_{i,wet}$ on dither-spectra $\Phi_{w_i}(\omega)$ is very marginal and its shape mostly dictated by the peripheral circuitry; however this implies that the actual plant input (used for direct identification) do vary significantly with $\theta_{i,wet}$, as explained by the relation $\Phi_{u_{w_i}}(\omega) = \left| \frac{F}{1+FCG} \right|^2 \Phi_{w_i}(\omega)$ derived from figure 2(b).

For predictor (17) in identification program (16) we used for open-loop covariances: $R = 10^{-2}$, $Q = I_{9\times 9}$, and for closed-loop: $R = 10^{-2}$, $Q = I_{10\times 10}$; Q dimensions defined through (8), (18).

B. Estimated T2R parameters

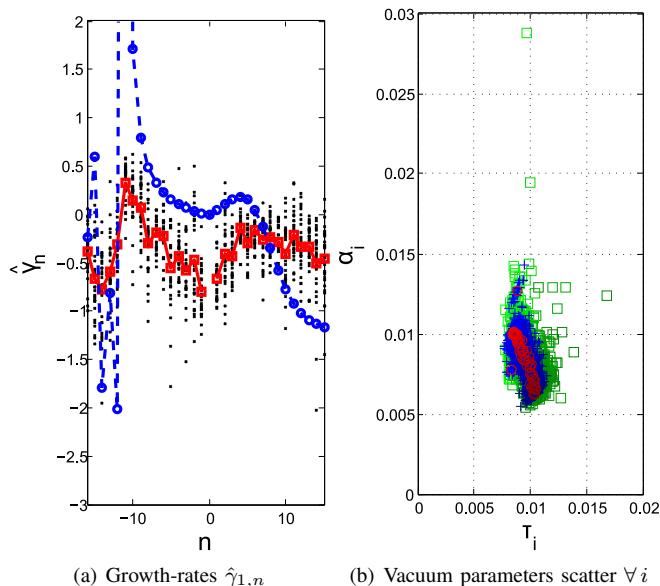(a) Growth-rates $\hat{\gamma}_{1,n}$ (b) Vacuum parameters scatter $\forall i$

Fig. 3. Estimated parameters for T2R. Plasma dataset: experiments #21804 − #21818.

Estimated RFP spectrum (red) of fig.3(a) exhibit similarities to theoretical shape (blue), a comforting result.

C. Implementational sidenote

A word of warning is issued to experimentalists. We felt we had to bin the real-time control computer's `rand()`-implementation for exactly this reason: generating 64 channels of ~ 1000 samples each clearly invalidates `RAND_MAX=16383` periodic pseudo-random sequence. The *minimal* implementation of [18] was invoked as a remedy.

VI. CONCLUSIONS

The immediate consequences of the minimalistic MHD normal modes dynamic description have been persued quite in depth by trying to engineer and execute *efficient* and *informative* experiments for external plasma response measurements and results do indicate, among other things, applicability of static decoupling methods for sparsification of the RWM control issue, for RFPs at least. For T2R, controller reconfigurations based on the results glimpsed at here, will be persued. The authors hope that this study can inspire tokamak researchers to adopt a related methodology.

ACKNOWLEDGEMENTS

REFERENCES

[1] M. Shimada *et al.*, "Progress in the ITER physics basis, chapter 1: Overview and summary," *Nuclear Fusion*, vol. 47, no. 6, pp. S1–S17, 2007. [Online]. Available: http://stacks.iop.org/0029-5515/47/S1

[2] J. Wesson, *Tokamaks*, 3rd ed., ser. International Series of Monographs on Physics. New York: Oxford Science Publications, 2004, no. 118.

[3] M. Walker *et al.*, "Emerging applications in tokamak plasma control: Control solutions for next generation tokamaks," *IEEE Control System Magazine*, vol. 26, pp. 35–63, 2006.

[4] H. Goedbloed and S. Poedts, *Principles of Magnetohydrodynamics*, 1st ed. Cambridge University Press, 2004.

[5] P. R. Brunsell *et al.*, "Feedback stabilization of multiple resistive wall modes," *Physical Review Letters*, vol. 93, no. 22, p. 225001, 2004. [Online]. Available: http://link.aps.org/abstract/PRL/v93/e225001

[6] "Controlled magnetohydrodynamic mode sustainment in the reversed-field pinch: Theory, design and experiments," *Fusion Engineering and Design*, vol. In Press, Corrected Proof, 2009.

[7] C. Bishop, "An intelligent shell for the toroidal pinch," *Plasma Physics and Controlled Fusion*, vol. 31, no. 7, pp. 1179–1189, 1989. [Online]. Available: http://stacks.iop.org/0741-3335/31/1179

[8] R. Fitzpatrick and E. P. Yu, "Feedback stabilization of resistive shell modes in a reversed field pinch," *Physics of Plasmas*, vol. 6, no. 9, pp. 3536–3547, 1999. [Online]. Available: http://link.aip.org/link/?PHP/6/3536/1

[9] D. Gregoratto *et al.*, "Studies on the response of resistive-wall modes to applied magnetic perturbations in the EXTRAP T2R reversed field pinch," *Physics of Plasmas*, vol. 12, no. 9, p. 092510, 2005. [Online]. Available: http://link.aip.org/link/?PHP/12/092510/1

[10] P. R. Brunsell, J.-A. Malmberg, D. Yadikin, and M. Cecconello, "Resistive wall modes in the EXTRAP T2R reversed-field pinch," *Physics of Plasmas*, vol. 10, no. 10, pp. 3823–3833, 2003. [Online]. Available: http://link.aip.org/link/?PHP/10/3823/1

[11] R. Paccagnella, D. Gregoratto, and A. Bondeson, "Feedback control of resistive wall modes in reversed field pinches," *Nuclear Fusion*, vol. 42, no. 9, pp. 1102–1109, 2002. [Online]. Available: http://stacks.iop.org/0029-5515/42/1102

[12] L. Ljung, *System Identification - theory for the user*, 2nd ed. Prentice-Hall, 1999.

[13] U. Forssell and L. Ljung, "Closed-loop identification revisited," *Automatica*, vol. 35, pp. 1215–1241, july 1999. [Online]. Available: http://dx.doi.org/10.1016/S0005-1098(99)00022-9

[14] B. D. O. Anderson and J. B. Moore, *Optimal filtering*, ser. Information and systems sciences. Prentice-Hall, 1979.

[15] R. F. Stengel, *Optimal control and estimation*. Dover Publications, 1994.

[16] H. Jansson, "Experiment design with applications in identification for control," Ph.D. dissertation, Royal Institute of Technology (KTH), dec 2004, TRITA-S3-REG-0404.

[17] R. A. Horn and C. R. Johnson, *Matrix Analysis*. Cambridge University Press, 1990.

[18] S. K. Park and K. W. Miller, "Random number generators: good ones are hard to find," *Commun. ACM*, vol. 31, no. 10, pp. 1192–1201, 1988.